Biosensors and Bioelectronics 46 (2013) 22–29

Contents lists available at SciVerse ScienceDirect

Biosensors and Bioelectronics

journal homepage: www.elsevier.com/locate/bios

Development of a label-free immunosensor based on surface plasmon resonance technique for the detection of anti-*Leishmania infantum* antibodies in canine serum

Dênio E.P. Souto [a,b,d], Jussara V. Silva [a], Helen R. Martins [b], Alexandre B. Reis [c], Rita C.S. Luz [a,d], Lauro T. Kubota [d], Flávio S. Damos [a,d,*]

[a] Instituto de Ciência e Tecnologia, Universidade Federal dos Vales do Jequitinhonha e Mucuri, 39100-000 Diamantina, MG, Brazil
[b] Departamento de Farmácia, Universidade Federal dos Vales do Jequitinhonha e Mucuri, 39100-000 Diamantina, MG, Brazil
[c] Departamento de Análises Clínicas, Universidade Federal de Ouro Preto, 35.400-000 Ouro Preto, MG, Brazil
[d] Instituto Nacional de Ciência e Tecnologia em Bioanalítica, Unicamp, 13083-970 Campinas, SP, Brazil

ARTICLE INFO

Article history:
Received 15 December 2012
Received in revised form
24 January 2013
Accepted 25 January 2013
Available online 20 February 2013

Keywords:
Leishmania infantum
Visceral leishmaniasis
Surface plasmon resonance
Immunosensor
Scanning electrochemical microscopy

ABSTRACT

In this work, a surface plasmon resonance (SPR) immunosensor was developed using an 11-mercaptoundecanoic acid (11-MUA) modified gold SPR sensor chip for the detection of anti-*Leishmania infantum* antibodies. The soluble antigens of *L. infantum* were securely immobilized on an SPR gold disk by an 11-MUA self-assembled monolayer. Cyclic voltammetry (CV), electrochemical impedance spectroscopy (EIS) and scanning electrochemical microscopy (SECM) techniques were employed in the characterization of the antigen immobilization. After the immunosensor construction, canine serum positive for visceral leishmaniasis was added to its surface and showed significant variation in the SPR angle, indicating excellent sensitivity of the technique for antigen–antibody interaction detection. Moreover, the addition of negative serum was accompanied by a smaller response, demonstrating that the immunosensor shows good specificity against anti-*L. infantum* antibodies. Therefore, this work demonstrates the successful development of an SPR sensor for anti-*L. infantum* antibodies detection in short time, showing a great perspective as a sensing system of visceral leishmaniasis in endemic regions.

1. Introduction

Leishmaniasis is a widespread zoonotic disease, which represents a serious public health problem with various clinical manifestations, depending on the *Leishmania* species (Lukes et al., 2007). According to disease-burden estimation, leishmaniasis is the second-ranking cause of mortality and the fourth-ranking in morbidity among neglected tropical diseases (Mathers et al., 2007). An estimated 12–15 million people are infected world-wide, with approximately 1.5–2 million new cases per year. Of these, about 500.000 are visceral leishmaniasis (VL) and 1.500.000 are cutaneous leishmaniasis (CL) (World Health Organization WHO, 2010). Whereas CL has a tendency to heal spontaneously and leave resulting scars, VL is fatal when left untreated, causing an estimated 59.000 deaths per year (35.000 men and 24.000 women) (Den Boer et al., 2011; Desjeux, 2004; Srivastava et al., 2011). Consequently, VL has aroused the concern of health authorities due to its appearance in large urban centers or its re-emergence in many cities around the world (Alves and Bevilacqua, 2004; Ashford, 2000).

VL is caused by species belonging to the *Leishmania donovani* complex. *L. donovani* and *Leishmania infantum* are the etiological agents found in the Old World, while only the latter is observed in the Americas (Murray et al., 2005). Dogs are considered the most important epidemiological reservoirs of *L. infantum* and serve as an abundant source of infection for the sandfly vector *Lutzomyia longipalpis*, due to its high skin parasitism (Reis et al., 2006). The large number of dogs infected in endemic areas carry the parasite to the insect vectors, constituting an important link in maintaining the transmission of infection to humans (Alves and Bevilacqua, 2004). Therefore, the diagnosis and euthanasia of positive dogs is essential to the success of controlling of LV (Moreno and Alvar, 2002).

The clinical aspects for diagnosing VL are a challenge, owing to nonspecific clinical signs and symptoms in oligosyntomatic and the high percentage of asymptomatic cases in humans and dogs (Teixeira-Neto et al., 2010). Thus, *a* definitive diagnosis depends on the laboratory tests, including parasitological and serological techniques, to confirm infection. Considering the high production of

* Corresponding author at: Instituto de Ciência e Tecnologia, Universidade Federal dos Vales do Jequitinhonha e Mucuri, 39100-000 Diamantina, MG, Brazil. Tel.: +55 38 3532 1283; fax: +55 38 3532 1223.
E-mail address: flavio.damos@ufvjm.edu.br (F.S. Damos).

0956-5663/$ - see front matter © 2013 Elsevier B.V. All rights reserved.
http://dx.doi.org/10.1016/j.bios.2013.01.067

anti-*L. infantum* antibodies during the course of an infection, the serological tests are currently recommended to make a VL diagnosis. The most common techniques are the enzyme-linked immunosorbent assay (ELISA), using crude antigen, and the indirect immunofluorescence assay (IFA), based on IgG antibodies.

However, cross reaction with other trypanosomatides, and low sensitivity to detect the asymptomatic cases, are the main limitations of these techniques. In addition, these tools are not easily adapted to large serological surveys of dogs in endemic areas because of the time involved in implementing and conducting the various steps (Teixeira-Neto et al., 2010). In order to improve canine diagnosis, simpler and faster, new approaches have been developed and validated but, currently, commercial rapid detection assay of anti-*Leishmania sp* antibodies in humans and animals has generally shown lower sensitivity and specificity when compared with ELISA and IFA (Andrade et al., 2009).

In this sense, the immunosensors have attracted great interest in recent years for the monitoring of biological and chemical agents in a variety of applications. Several signal-transduction platforms have recently been developed, such as electrochemical impedance spectroscopy (EIS)-based immunosensors (Gamero et al., 2010; Im et al., 2010; Venugopal et al., 2011), Quartz crystal microbalance (QCM)-based immunosensors (Buchatip et al., 2010; Chen et al., 2011; Salmain et al., 2011) and surface plasmon resonance (SPR)-based immunosensors (Arya et al., 2011; Hong et al., 2011; Liu et al., 2011). Among them, SPR-based sensors have been widely recognized as a potential analytical tool due to their extreme sensitivity to small changes in the refractive index near to the sensor surface caused by the variation of the mass on the transducer surface. SPR requires neither label nor tracer, thus reducing the number of steps while allowing for the analysis of biomolecular interactions in real time. Furthermore, the SPR technique permits the investigation of kinetics and thermodynamic parameters and also the regeneration of the sensor surfaces and low cost analysis.

The procedure for the immobilization of biomolecules is essential, since the species to be immobilized must keep their properties for recognition, to develop an efficient SPR-based immunosensor. Thus, the use of self-assembled monolayers (SAMs) as an initial step for preparation of biosensors has provided greater sensitivity and stability to these systems (Cancino and Machado, 2012).

A SPR based-immunosensor was developed for direct and highly sensitive detection of anti-*L. infantum* antibodies through the *L. infantum* antigens immobilized on SAM of 11-MUA on the gold substrate. SECM was used for 2-D electrochemical imaging of *L. infantum* antigens immobilized on SAM of 11-MUA on the gold substrate. To our best knowledge, this is the first SPR-based immunosensor for anti-*L. infantum* antibodies detection.

2. Materials and methods

2.1. Reagents and chemicals

11-MUA, N-hydroxysuccinimide (NHS), N-(3-Dimethylaminopropyl)-N-ethylcarbodiimidehydrochloride (EDC), 4-(2-hydroxyethyl) piperazine-1-ethanesulfonic acid (Hepes) and ethanolamine (EA) were purchased from Sigma-Aldrich Chemical (St. Louis, MO, USA). Ethylenediamine tetraacetic acid (EDTA), NaCl, KCl and HCl were purchased from Isofar (Rio de Janeiro, Brazil). Tween 20 (surfactant P20) and KOH were obtained from Vetec Química Fina LTDA (RJ, Brazil). Ethanol (99.5%) and monobasic sodium phosphate were purchased from Dinâmica® Química (São Paulo, Brazil).

HBS-EP pH 7.4 buffer solutions were obtained by mixing solutions of 10.0 mmol L^{-1} Hepes pH 7.4, 3.0 mmol L^{-1} EDTA pH 8.0, 150.0 mmol L^{-1} NaCl and 0.005% surfactant P20. All solutions were prepared with water purified in a Milli-Q system. The ethanolic solution of 11-MUA was freshly prepared with ethanol before using, and all chemicals were of analytical grade and used as received.

2.2. Apparatus

Cyclic voltammetry (CV), differential pulse voltammetRy (DPV) and electrochemical impedance spectroscopy (EIS) were carried out with an AUTOLAB PGSTAT 128N Potentiostat/Galvanostat from *Eco Chemie B.V.*, (the Netherlands). For these measurements a cell with capability of 10 mL, with an Ag/AgCl electrode (KCl 3.0 mol L^{-1}) as reference electrode, a platinum wire as counter electrode and gold film of sensor disc as working electrode (0.0314 cm^2) were used.

SECM measurements were carried out using a CHI-920C scanning electrochemical microscope (CH Instrument, Austin, TX, USA) that uses a combination of stepper motors and an XYZ piezo block in order to position the UME (ultramicroelectrode). A four-electrode electrochemical cell was used, a Pt UME as first working electrode (Tip), a gold SPR disk as the second working electrode (substrate), a Pt wire as the counter electrode and an Ag/AgCl (3 mol L^{-1} KCl) as the reference electrode. All potentials are reported with respect to this reference throughout the manuscript. The SECM approach curves were obtained at 10 μm diameter Pt tip sealed with glass. The RG value (RG is the ratio of the radius of insulating sheath (*rg*) to the radius of conductive disk (*a*), so that RG=*rg*/*a*) of the tips used in this work were obtained at about 10.

Approach curves were recorded by moving the tip toward the surface of gold SPR disk at the speed of 2.5 μm s^{-1}, while the tip was held at a constant potential for a diffusion-limited current of solution-phase probe at the tip. For kinetic measurements, a family of approach curves, obtained at different substrate potentials, was fitted to theory to yield kinetic electron transfer constant (k_{ET}) values using the analytical approximation method for fitting approach curves described by Bard (Wei et al., 1995).

The biomolecular interactions were investigated using an SPR system Autolab Springle from *Eco Chemie B.V.*, (the Netherlands), in which the optical system comprises a glass prism and a planar gold SPR disk, both purchased from Metrohm-Autolab. The flow rate and temperature of the SPR system were maintained at 48 μl/min and 23 ± 1 °C, respectively, during the measurements. It functions with a laser diode fixed at a wavelength of 670 nm, using a vibrating mirror to modulate the angle of incidence of the p-polarized light beam on the SPR substrate. The instrument is equipped with a cuvette and based on the Kretschmann configuration, which is also the most commonly used configuration in SPR.

2.3. Production of soluble antigens of Leishmania infantum

The present study employed soluble antigens obtained from promastigotes of *L. infantum* (MHOM/BR/1070/BH46). Promastigotes were harvested in an LIT (Liver Infusion Tryptose) medium. The parasites were washed three times by centrifugation in phosphate buffer solution (PBS) at pH 7.2, for 10 min. After, the parasites were disrupted with three 1-min cycles at 40 W ultrasound (Sonifier® Cell Disruptor—Branson Sonic Power Co., USA) in an ice bath. Sonicated culture material was then centrifuged at 37,000 × *g* for 1 h and 30 min at 4 °C. The supernatant was transferred to dialysis tubes and dialyzed through PBS for 24 h at 4 °C. The remaining material was filtered in disposable sterile 0.22 μm filters (Millipore Co., Massachusetts, USA) under aseptic conditions, and a single aliquot was removed for protein dosage. Finally, the concentration was adjusted to 1.0 mg mL^{-1} and antigen samples in aliquot were frozen at −80 °C until use.

2.4. Canine serum

The canine serum samples were obtained from dogs naturally infected with *L. infantum* from endemic regions, with diagnoses established by the Secretary of Health in the city of Belo Horizonte, Brazil, and confirmed in the laboratory of Immunopathology at the Federal University of Ouro Preto (UFOP), Ouro Preto, Minas Gerais, Brazil. In addition, sera from healthy mongrel dogs housed in non-endemic regions (those raised in the Animal Center of the Federal University of Ouro Preto) were used as controls. The collection of these samples was approved by the ethics committee on research/UFOP, project number 2007/83.

2.5. The formation of 11-MUA SAM on the gold surface

The cleaning of the bare gold surface is of critical importance for self-assembled monolayer formation and should be done accomplished systematically. The gold electrode was immersed in a piranha solution (1:3 mixture of 30% H_2O_2–H_2SO_4 conc.) for 3 min. The surface was then washed copiously with water. After that, the gold films were immersed in absolute ethanol solution consisting of 11-MUA in different concentrations (0.1, 1.0 and 10.0 mmol L^{-1}) during different immersion periods (0.5, 2, 8, 16, 24 and 60 h). After optimization of these parameters, the gold films were rinsed several times with ethanol and water. After that, the gold films were dried with pure N_2 stream. In the next step SAM was activated by introducing NHS–EDC reagent (aqueous solution of 150 mmol L^{-1} NHS and 100 mmol L^{-1} EDC) for approximately 15 min. The sensor disc was rinsed in HBS-EP buffer at pH 7.4, and immediately after it was attached to the prism of the SPR instrument and activated SAM on sensor disc was ready. The SPR angle was monitored until the baseline stabilization.

2.6. Antigen immobilization on the sensor

The immobilization of the soluble *L. infantum* antigens on the activated 11-MUA SAM was carried out in the SPR system. In this step various concentrations of *L. infantum* antigen (10, 18, 30, 40 and 50 μg mL^{-1}) were investigated, as well as different immobilization periods of these antigens on the sensor disc (1, 5, 10, 30 and 60 min), were studied. After the establishment of the baseline by the addition of 200 μL of HBS-EP buffer at pH 7.4, 100 μL of *L. infantum* antigen dissolved in HBS-EP buffer at pH 7.4 was injected in the cell. Then, a covalent crosslinking by amino reactive group of antigen with the ester terminals was achieved. After that, the immunosensor was thoroughly rinsed with HBS-EP buffer at pH 7.4 to remove the excess of unbounded material. At following, the unbound reactive ester groups were deactivated by a brief flow of 100 mmol L^{-1} ethylenediamine (EA) solution for about 5 min to prevent non-specific binding.

2.7. Detection of the immunoreaction between soluble antigens of *L. infantum* and anti-*L. infantum* antibodies using the SPR technique

In order to evaluate the diagnostic capability of the developed immunosensor, 20 canine sera were employed: 10 which were negative for visceral leishmaniasis (VL) and 10 which were positive. These canine sera were used for preparing a pool of animals both positive and negative to VL. Sera were prepared with different dilutions (1:50, 1:100, 1:400, 1:800, 1:1600, 1:3200, 1:6400, 1:12800, 1:25600, 1:51200 and 1:102400) in HBS-EP buffer at pH 7.4. For each dilution factor mentioned, were injected 200 μL on the immunosensor. The immunoreaction between immobilized antigen and antibody (the association phase) was studied for different periods (60, 300, 600, 1800 and 3600 s). An optimum time period of 600 s was found to be satisfactory to get a stable SPR signal for successful interaction and binding of reaction product onto the sensor surface. Every association phase was followed by a brief flow of carrier HBS-EP buffer at pH 7.4 to wash away the unreacted/loosely bound species (the dissociation phase).

3. Results and discussion

3.1. Evaluation of *L. infantum* antigens immobilization

In order to immobilize the *L. infantum* antigens, the characteristics of 11-MUA SAM produced by the adsorption of 11-mercaptoundecanoic acid on a gold-coated glass SPR sensor disk were evaluated. In this sense, under optimized conditions, 11-MUA (1.0 mmol L^{-1}) ethanolic solution and a 24-h immersion period of gold substrate were sufficient for stable SAM formation on the gold surface. To obtain further information and control regarding the SAM characteristics, the dielectric constant (ε) and thickness (d) of the thiol film adsorbed on the gold substrate were investigated through SPR (Bruijn et al., 1991). The values found for ε and d were 2.17 and 13.3 Å, respectively, for surface coverage Γ of 26.6 10^{-12} mol cm^{-2}, which are in agreement to the literature (Bruijn et al., 1991; Zhang et al., 2009) indicating a good quality in 11-MUA SAM formation.

For the covalent protein immobilization, the COOH terminal groups in 11-MUA SAM were activated previously with coupling agents (EDC/NHS) followed by immersion in PBS-EP solution (pH 7.4), and the resonant angle was monitored until the baseline stabilization. As shown in Fig. 1A, the injection of *L. infantum* antigen in the SPR cuvette containing the NHS/EDC-activated 11-MUA SAM produced an increase in the local dielectric constant, resulting in an increase of 180 millidegrees (m°) in the SPR angle due to the antigen immobilization. This procedure led to the formation of amide bonds between the NHS ester group on the activated surface and *L. infantum* antigen, which contained reactive amine groups (Löfas and Whirter, 2006). Subsequently, the *L. infantum* antigen-modified sensor surface was cleansed with HBS-EP buffer at pH 7.4 (Fig. 1A) to wash off the nonspecific bound antigen. The change of the resonant angle was monitored and the signal was calculated from the SPR angles after the washing procedure.

After optimizing the conditions for preparing the immunosensor, the signal relationship with respect to the *L. infantum* antigen concentration is presented in Fig. 1B. As shown by the inset figure, the shift in the SPR angle also increased in proportion to the concentration of *L. infantum* antigen, thereby presenting a linear relationship between the concentration of antigen and the shift of SPR angle after the interaction time of about 30 min.

These results indicate the efficiency of the 11-MUA SAM produced for *L. infantum* antigen immobilization, since the addition of antigen in the absence of SAM was not accompanied by displacement of the SPR angle ($\Delta\theta_{SPR}$), noting that the process of soluble *L. infantum* antigen immobilization was highly stable on the sensor disc.

3.2. Characterization of immunosensor by cyclic voltammetry (CV), electrochemical impedance spectroscopy (EIS) and scanning electrochemical microscopy (SECM)

CV, EIS and SECM techniques were used to characterize the *L. infantum* antigens on SAM. The redox couple $Fe(CN)_6^{3-/4-}$ was preferred for use as an electrochemical probe for examining the integrity of SAM on gold (Kiani et al., 2008). Fig. 2 shows cyclic voltammograms of the bare gold electrode (curve 1), the stepwise

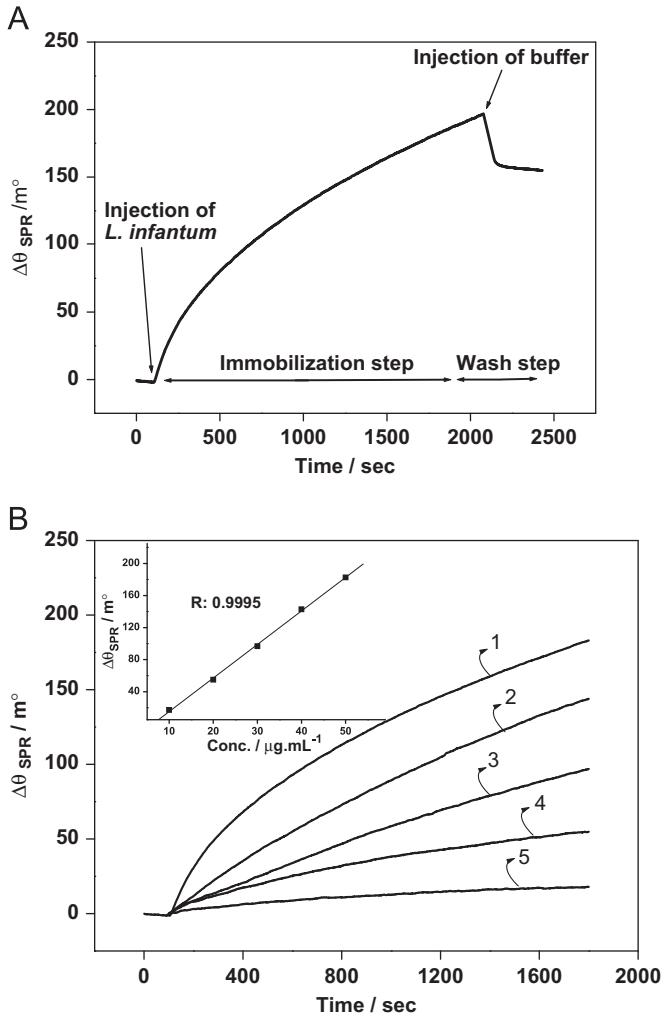

Fig. 1. Sensograms regarding the immobilization of soluble *L. infantum* antigens in HBS-EP buffer pH 7.4 onto the activated self-assembled 11-MUA. (A) Immobilization and washing steps of the antigen (50 μg mL^{-1}). (B) Immobilization steps for the antigen at different concentrations: 10 μg mL^{-1}; 20 μg mL^{-1}; 30 μg mL^{-1}; 40 μg mL^{-1} and 50 μg mL^{-1}, curves 1, 2, 3, 4, and 5, respectively. Inset: a linear relationship between the concentration of antigen and the SPR angle shift, after an adsorption time of about 30 min.

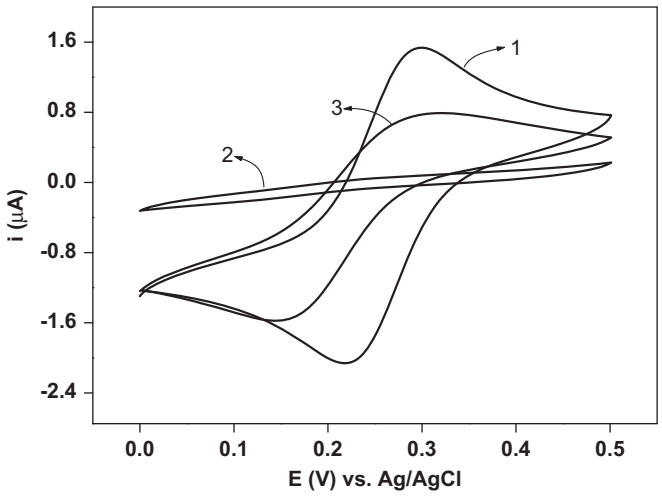

Fig. 2. Cyclic voltammograms obtained for the aqueous solution $Fe(CN)_6^{3-/4-}$ (1 mmol L^{-1}) redox reaction on the bare gold electrode (curve 1), on 11-MUA (1.0 mmol L^{-1}) ethanol solution after a modification time of 24 h (curve 2) and after antigen immobilization on SAM (curve 3). The measurements were performed in 0.1 mol L^{-1} KCl and a scan rate of 20 mV/s.

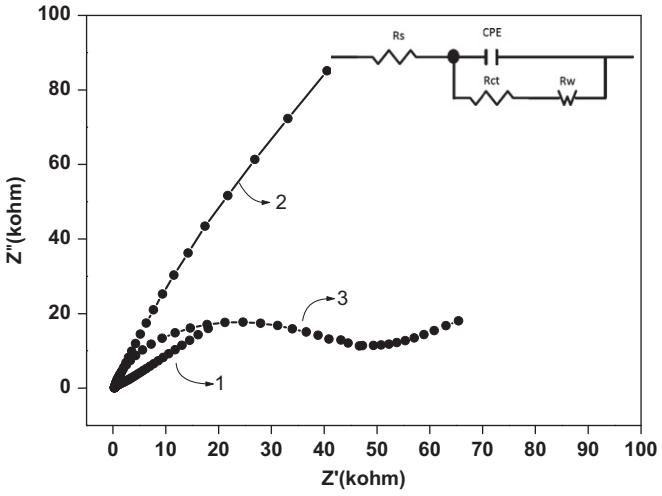

Fig. 3. (A) Nyquist plots (Z'' vs Z') of a bare gold electrode (curve 1), an MUA SAM modified gold electrode (curve 2) and an *L. infantum* antigen/MUA SAM modified gold electrode (curve 3) in a KCl solution (0.1 mol L^{-1}) containing 1.0 mmol L^{-1} $Fe(CN)_6^{3-/4-}$. The inset is the equivalent circuit applied to model impedance spectra data in the presence of the redox probe. R_s, R_W, R_{ct} and CPE represent the solution resistance, the Warburg diffusion resistance, the charge-transfer resistance and the constant phase element, respectively.

attachment of 11-MUA after an adsorption time of 24 h (curve 2), and the adsorption of *L. infantum* antigens onto the activated self-assembled 11-MUA (curve 3).

As can be seen, two well-defined peaks characteristic of $Fe(CN)_6^{3-}/Fe(CN)_6^{4-}$ were observed on the bare gold electrode. However, the 11-MUA SAM/Au surface resulted in preventing the access of the $Fe(CN)_6^{3-}/Fe(CN)_6^{4-}$ redox species to the electrode. Hence, no Faradaic peaks for $Fe(CN)_6^{3-}/Fe(CN)_6^{4-}$ were observed between 0.0 V and +0.5 V vs Ag/AgCl. On the other hand, an increase in the peak current of the redox couple was observed after the incubation of the 11-MUA/Au electrode surface with *L. infantum* antigens. EIS is a sensitive and powerful characterization tool that can provide detailed information on charge-transfer resistance (R_{ct}), which reflects the electron transfer kinetics of the redox probe at the electrode surface (Luz et al., 2005; Pei et al., 2001).

Fig. 3 shows the Nyquist plots of the bare gold electrode (curve 1), the MUA SAM modified gold electrode (curve 2) and the *L. infantum* antigen/MUA SAM modified gold electrode (curve 3) in the presence of the redox probe measured at the formal potential. The measured EIS data were simulated with a modified Randles equivalent circuit as shown in inset of Fig. 3. This circuit consists of the ohmic resistance of the electrolyte (R_s) between the gold working electrode and the Ag/AgCl reference electrode, R_{ct} of the redox probe moving through the film, the Warburg impedance (R_w) resulting from the diffusion of ions from the bulk of the electrolyte to the interface and a constant phase element (CPE) is used instead of a pure capacitor to compensate for the non-ideal capacitive response of the interface (Ding et al., 2005; Hleli et al., 2006; Norlin et al., 2002; Randles, 1947).

The bare gold electrode exhibits an almost straight line with a small semicircle at high frequencies (Fig. 3, curve 1), indicating a diffusion-limited electron transfer process (R_{ct}=2.90 kΩ). After immobilization of the MUA, the value of R_{ct} increased to 1600 kΩ (Fig. 3, curve 2), which indicated the successful formation of a MUA SAM, thus blocking the electron transfer of the redox probe to the electrode surface. After immobilization of the *L. infantum* antigen on MUA SAM, the R_{ct} decayed to 43.2 kΩ, confirming the

trend observed in cyclic voltammetry experiments. It is possible that the antigen immobilization on SAM caused defects in the structure of the monolayer, thus decreasing the electron transfer resistance at the surface. Indeed, the terminal carboxylic group of MUA is negatively charged in the pH solution (pH 7.4). The redox probe of $[Fe(CN)_6]^{3-/4-}$ was also negatively charged, and thus the redox probe was difficult to approach on the electrode surface due to the strong electrostatic repulsion. After activation with EDC/NHS, the majority of terminal carboxylic groups were converted to NHS esters, so that repulsive interaction with the anionic probe $[Fe(CN)_6]^{3-/4-}$ at the electrode interface did not occur, thus promoting the transfer of the redox ions $[Fe(CN)_6]^{3-/4-}$ to the electrode surfaces. It was observed that the monolayers became less insulating, and that an increase in current response occurred.

The constant phase element values were extracted from computer simulated spectra which are 7.89 μF cm^{-2}, 0.954 μF cm^{-2} and 0.450 μF cm^{-2} for the bare gold electrode, MUA SAM and *L. infantum* antigen/MUA SAM, respectively. It is well known that long-chain alkanethiols, such as MUA, form very well ordered defect-free monolayers, which constitute a barrier to the electron transfer and the penetration of ions towards the electrodic substrate (Campuzano et al., 2006). Thus, when a MUA SAM with a long alkane chain is deposited on an electrode surface, the interfacial capacitance was 0.954 μF cm^{-2}, value that is more than 8-fold lower than the characteristic capacitance of bare gold electrode.

Scanning electrochemical microscopy (2-D imaging and approach curves) measurements were carried out in order to investigate the effects of electrostatic repulsion between the redox couple and the films, as well as the defects in the MUA SAM and *L. infantum* antigen/MUA SAM on the electron transfer of the redox probe to the electrode surface. Thus, the SECM experiments were performed for the MUA SAM modified gold electrode and the *L. infantum* antigen/MUA SAM modified gold electrode in the presence of hydrophilic species of $[Fe(CN)_6]^{4-}$.

Fig. 4 shows the SECM approach curves of $[Fe(CN)_6]^{3-/4-}$ on the MUA SAM modified gold electrode (Fig. 4A) and the *L. infantum* antigen/MUA SAM modified gold electrode (Fig. 4B). Approach curves were collected as a function of substrate potential, while the tip potential was set to the value at which the diffusion-controlled oxidation of the probe $[Fe(CN)_6]^{4-}$ could occur at tip (E_{tip}=0.5 V vs Ag/AgCl) and the substrate potential was **s**tepped to greater negative values progressively. This procedure was carried out in the same region on the substrate to obtain a family of effective heterogeneous electron transfer constants, k_{eff}, values as a function of substrate potential. According to the theory, the following equations can be used to extract the first order k_{eff} (Mirkin et al., 1992; Wei et al., 1995):

$$I_T^k = I_S^k\left(1-\frac{I_T^{ins}}{I_T^C}\right)+I_T^{ins} \quad (1)$$

$$I_S^k = \frac{0.78377}{L(1+1/\Lambda)}+\frac{[0.68+0.3315\exp(-1.0672/L)]}{[1+F(L,\Lambda]} \quad (2)$$

where I_T^C, I_T^k, I_T^{ins} represent the normalized tip current for diffusion-controlled regeneration of the redox mediator, finite substrate kinetics, and insulating substrate, respectively, at a normalized tip-substrate separation, $L=d/a$; I_T^k is the kinetically controlled substrate current; and $\Lambda=k_{ET}d/D$, where k_{ET} is the apparent heterogeneous rate constant (cm/s), and $F(L,\Lambda)=(11+2.3\Lambda)/[\Lambda(110-40L)]$. These currents are normalized by the tip current at an infinite tip-substrate separation, $i_{T,\infty}$. The analytical approximations for I_T^C and I_T^{ins} (Mirkin et al., 1992; Wei et al., 1995)

$$I_T^C = \frac{0.78377}{L}+0.3315\exp\left(-\frac{1.0672}{L}\right)+0.68 \quad (3)$$

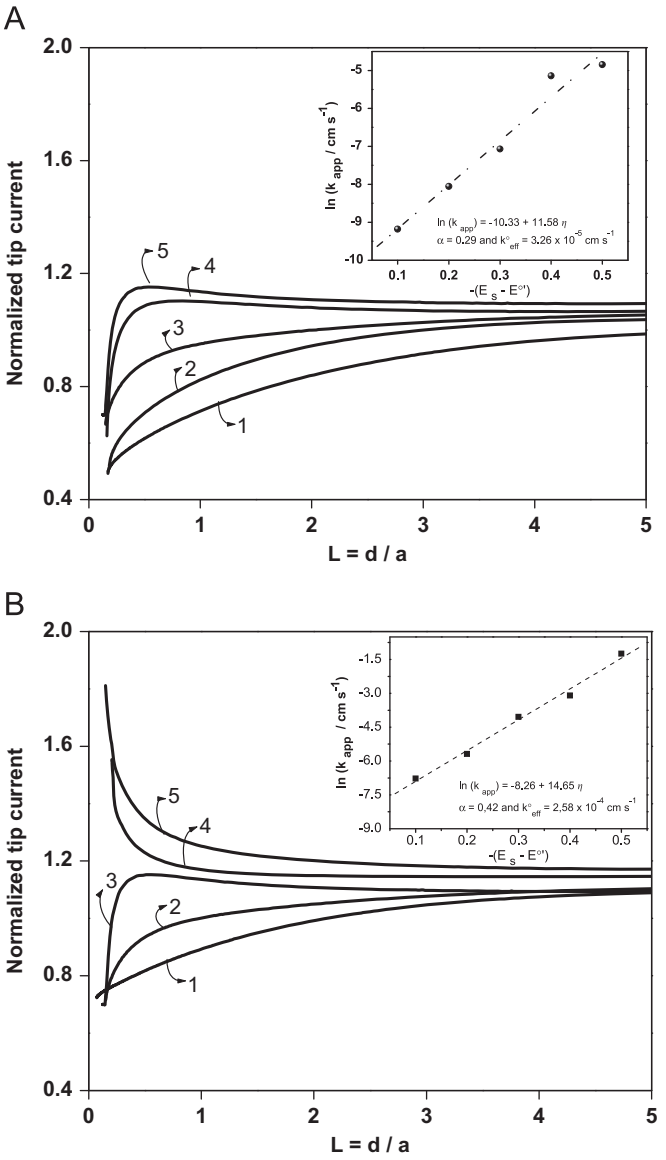

Fig. 4. SECM approach curves obtained on a gold electrode coated by (A) MUA SAM and (B) *L. infantum* antigen/MUA SAM, in a solution containing 1 mmol L^{-1} $[Fe(CN)_6]^{4-}$ and 0.1 mol L^{-1} KCl. The tip was a 10 μm diameter Pt disk. The Tip was polarized at 0.5 V and the substrate overpotentials were (1) −0.1, (2) −0.2, (3) −0.3, (4) −0.4 and (5) −0.5 V vs Ag/AgCl. Scan rate=2.5 μm s^{-1}. The insert shows the measurement rate constant for MUA SAM (A) and antigen/MUA SAM (B). Lines show the data fitted to buffer—the Volmer theory in Fig. 4.

$$I_T^{ins} = \frac{1}{0.15+1.5358/L+0.58\exp(-1.14/L)+0.0908\exp[L-6.3/1.017L]} \quad (4)$$

Effective heterogeneous electron transfer constants for the MUA SAM modified gold electrode and the *L. infantum* antigen/MUA SAM modified gold electrode were obtained with 1 mmol L^{-1} of $[Fe(CN)_6]^{4-}$. For blocking monolayers, the rate constants at one region of the substrate were fit to the Buttler–Volmer equation to obtain both the heterogeneous rate constant, k_{ET}°, and the electron transfer coefficient, α (Kiani et al., 2008)

$$k_{ET} = k_{ET}^{o}\exp[-af(E_s-E^o)] \quad (5)$$

where $f=F/RT$, F is the Faraday constant, R is the gas constant and T is the temperature.

It can be seen in Fig. 4 that in the case of the *L. infantum* antigen/MUA SAM modified gold electrode, deviation from pure

negative feedback begins at lower potentials compared to that of the MUA SAM modified electrode. Indeed, the k_{ET} values obtained were higher for *L. infantum* antigen/MUA SAM compared to MUA SAM, which is consistent with cyclic voltammetry and electrochemical impedance experiments. As substrate potential varied, the rate of the redox couple oxidation through the SAM increased, and the approach curves change from negative to positive feedback. The rate constants obtained were fit to Eq. (5) and a k_{ET}° value of 3.26×10^{-5} cm s^{-1} and a α value of 0.29 were obtained for MUA SAM (see inset in Fig. 4A) and a k_{ET}° value of 2.58×10^{-4} cm s^{-1} and a α value of 0.42 were obtained for *L. infantum* antigen/MUA SAM (see inset in Fig. 4B).

Images of electrochemical reactivity for the probe (1.0 mmol L^{-1} ferrocyanide in 0.1 mol L^{-1} KCl) across the substrate were also obtained by SECM. Scanning in a rastered pattern was performed at a constant substrate-tip separation above the tooth sample. All the images presented in this paper relate to a 300 μm × 300 μm area of the substrate. The micro-electrode and the substrate were polarized at 0.5 V and 0.0 V vs Ag/AgCl, respectively. The SECM images in Fig. 5 correspond to a 2-D representation of the local tip current after approach in substrate, consisting, respectively, of 11-MUA SAM (Fig. 5A) and of antigens immobilized on 11-MUA SAM (Fig. 5B). By comparing images (A) and (B) in Fig. 5, it can be seen that the results observed in this study clearly demonstrate that after immobilization of antigens on the surface, there was an increase in the current obtained from the electrochemical redox reaction of the probe used, confirming the data found by the CV and EIS techniques, as well as the kinetic data from SECM.

3.3. Immunosensor response to anti-*L. infantum* antibodies

The efficiency of the SPR-based immunosensor was evaluated by adding to its surface of positive and negative canine sera for VLC. Fig. 6A shows the sensogram obtained for the steps involved in the detection of anti-*L. infantum* antibodies. In first step, stabilization of baseline was performed for 180 s. In second step, the immobilization of the *L. infantum* antigen onto the activated 11-MUA SAM is evidenced by a rise in the resonance angle (position 1, Fig. 6A). In third step, washing was performed with HBS-EP buffer at pH 7.4 (position 2, Fig. 6A) and in fourth step, to prevent non-specific binding and also for the blocking of unreacted NHS-ester groups on sensor chip, EA was used (position 3, Fig. 6A) followed by a brief wash with HBS-EP buffer at pH 7.4 (position 4, Fig. 6A) to remove unbound species from the sensor surface. In the fifth step, the immunoreaction between the *L. infantum* antigen and the anti-*L. infantum* antibody, after injection of positive canine serum at 1:50 dilution, was monitored (position 5, Fig. 6A). An interaction time of 10 min showed a strong antigen–antibody interaction, as evidenced by a sharp rise in resonance angle shift of about 600 m°, demonstrating a very high sensitivity of the proposed label-free immunoassay. After measuring the immune response, the regeneration step was carried out using 1% (w/v) sodium dodecyl sulfate (SDS) prepared in water and a pulse of about 3 min, which was found appropriate to liberate the bound antigen–antibody, leaving the sensor surface active for the next injection. In inset of Fig. 6A, the SPR sensorgrams shows four repeated injections of positive canine serum of *L. infantum* antibody and regenerated surface with 1% (w/v) SDS. The heights of the SPR sensorgrams were almost the same and we observed no reduction in the response. The relative standard deviation in the SPR angle for the four measurements was 4%.

Positive canine serum in different dilutions was subsequently injected onto the immunosensor surface. The sensorgrams showed in Fig. 6B involves association step due to interaction antigen–antibody. The sensitivities of the immunosensors prepared with

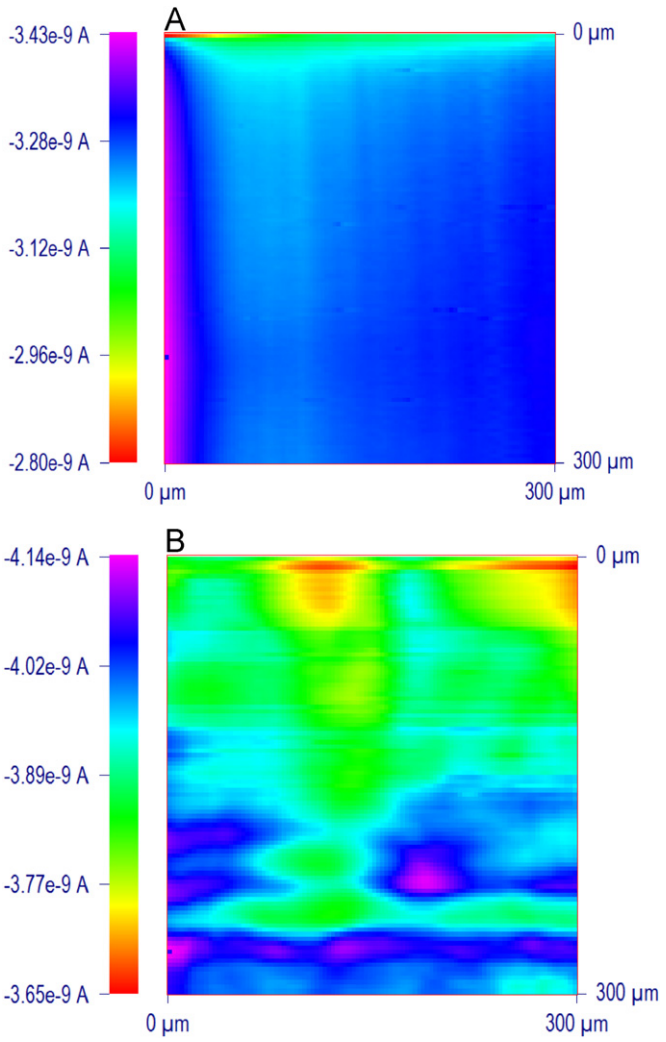

Fig. 5. SECM 2-D images obtained with a platinum microelectrode (r=5 μm) in 1.0 mmol L^{-1} $Fe(CN)_6^{3-/4-}$ in the presence 0.1 mol L^{-1} KCl for an substrate consisting of 11-MUA (1.0 mmol L^{-1}) (A) and consisting of antigen (50 μg mL^{-1}) immobilized on SAM (B). Scan rate: 3.0 μm s^{-1}.

different amounts of anti-*L. infantum* antibodies were presented. It is possible to observe in Fig. 6B the wide detection range and excellent sensitivity of anti-*L. infantum* through immunosensor construction and also note that at lower concentrations of antibodies (or larger dilutions of serum), the immunosensor sensitivity is reduced, due to the low number of interactions of antibodies on the immunosensor. Calibration plot was constructed using the logarithm of $\Delta\theta_{SPR}$ against dilution of positive canine sera and the figure is presented in Fig. 6C. The calibration plot exhibited the linearity over the dilution range of 1:6400–1:50 with a value of 0.995 correlation coefficient.

Moreover, the addition of negative serum in different dilutions (1/50–1/6400) was accompanied by a smaller response when compared with positive serum. Even more significant differences for sera with dilution factor greater than 200 were obtained. Currently the Ministry of Brazilian Health formally establishes that an animal is reagent considered when dilution factor shows equal or superior to 1:40 in ELISA and IFA, but this criterion is still controversy considering that for several authors only the dilution factor equal or higher that 1:160 should be conclusive considered. However, in this dilution factor the failure in demonstrating the infection by ELISA and IFA in asymptomatic dogs is more marked and the higher dilution can also show loss of specificity. In this sense, the results obtained by our group indicate the successful in

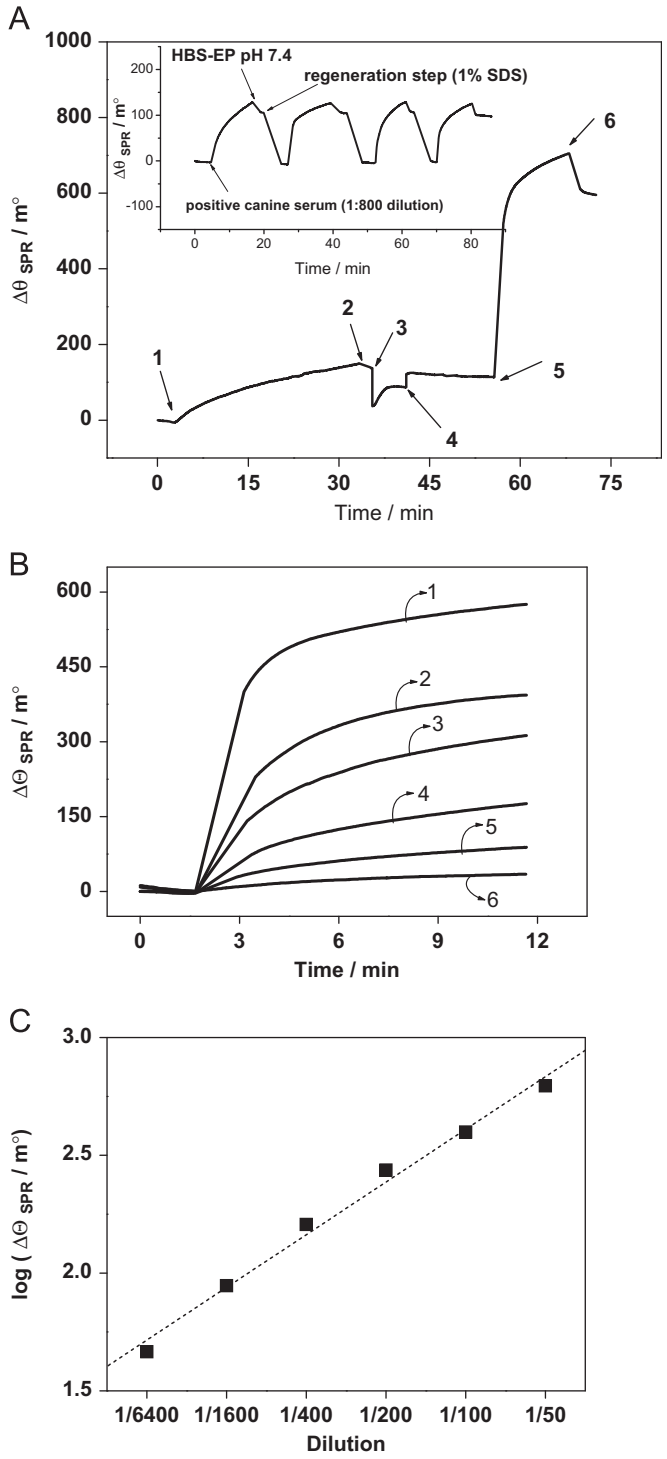

Fig. 6. (A) Sensogram showing the immobilization and immunoreaction of *L. infantum* antigen onto the activated 11-MUA modified gold surface [position 1, injection of *L. infantum* antigen (50 μg mL^{-1}); position 2, 4, 6, HBS-EP pH 7.4 buffer flow; position 3, injection of EA; position 5, injection of positive canine serum at 1:50 dilution]. Inset: SPR sensorgrams observed when positive canine serum of *L. infantum* antibody was injected repeatedly after regeneration carried out using 1% (w/v) SDS. (B) Curves obtained due to the injections of positive canine serum in different dilutions (v/v): 1:50, 1:100, 1:200, 1:400, 1:1600 and 1:6400 (curves 1, 2, 3, 4, 5 and 6, respectively) on the immunosensor. (C) Calibration plot for the interaction of different dilutions of positive canine sera with immobilized *L. infantum* antigen.

the development of an SPR-based sensor, indicating advantages when compared to conventional techniques, such as, excellent sensitivity for anti-*L. infantum* antibodies detection, short time analysis and real time detection. Therefore, the SPR-based immunosensor prepared shows a great perspective as a sensing system to the diagnosis of VLC.

4. Conclusions

The development of an immunosensor for anti-*L. infantum* antibodies detection by the SPR technique was successfully performed. The sensor showed good response, allowing analysis of interactions in real time and without needing markers, showed a great perspective as a sensing system to VLC in endemic regions. The SPR immunosensor based on the *L. infantum* antigen was successfully applied to the analysis of antibodies against anti-*L. infantum* antibodies in canine serum up to 1: 1:6400 diluted. Area scans with SECM (2-D imaging and approach curves) clearly demonstrate that after immobilization of antigens on the surface, there was an increase in the current obtained from the electrochemical redox reaction of the probe used, confirming the data found by the CV and EIS techniques.

Acknowledgments

The authors are grateful to Conselho Nacional de Desenvolvimento Científico e Tecnológico (CNPq), INCTBio, Fundação de Amparo à Pesquisa do Estado de Minas Gerais (FAPEMIG) and Fundação de Amparo à Pesquisa do Estado de São Paulo (FAPESP) for financial support. D. E. P. S is indebted to INCT-Bio for fellowships.

References

Alves, W.A., Bevilacqua, P.D., 2004. Cadernos de Saúde Pública 20, 259–265.
Andrade, R.A., Araújo, M.S.S., Reis, A.B., Gontijo, C.M.F., Vianna, L.R., Mayrink, W., Martins-Filho, O.A., 2009. Veterinary Immunology and Immunopathology 128, 79–86.
Arya, S.K., Singh, A.T., Naidoo, R., Wu, P., Mcdermott, M.T., Eyoy, S., 2011. Analyst 136, 486–492.
Ashford, R.W., 2000. International Journal for Parasitology 30, 1269–1281.
Bruijn, H.E., Altenburg, B.S., Kooyman, R.P.H., Greve, J., 1991. Optics Communications 82, 425–432.
Buchatip, S., Ananthanawat, C., Sithigorngul, P., Sangvanich, P., Rengpipat, S., Hoven, V.P., 2010. Sensors and Actuators B 145, 259–264.
Campuzano, S., Pedrero, M., Montemayor, C., Fatás, E., Pingarrón, J.M., 2006. Journal of Electroanalytical Chemistry 586, 112–121.
Cancino, J., Machado, S.A.S., 2012. Electrochimica Acta 72, 108–113.
Chen, J.-C., Sadhasivam, S., Lin, F.-H., 2011. Process Biochemistry 46, 543–550.
Den Boer, M., Argaw, D., Jannin, J., Alvar, J., 2011. Clinical Microbiology and Infection 17, 1471–1477.
Desjeux, P., 2004. Clinical Microbiology and Infection 27, 305–318.
Ding, S.J., Chang, B.W., Wu, C.C., Lai, M.R., Chang, H.C., 2005. Electrochimica Acta 50, 3660–3666.
Gamero, M., Pariente, F., Lorenzo, E., Alonso, C., 2010. Biosensors and Bioelectronics 25, 2038–2044.
Hleli, S., Martelet, C., Abdelghani, A., Burais, N, Jaffrezic-Renault, N., 2006. Sensors and Actuators B 113, 711–717.
Hong, S.C., Chen, H., Lee, J., Hye-Kyung, P., Young, S.K., Hyun-Chul, S., Cheol-Min, K., Tae, J.P., Seok, J.L., Kwangnak, K., Hwa-Jung, K., Chulhun, L.C., Jaebeom, L., 2011. Sensors and Actuators B 156, 271–275.
Im, J.-E., Han, J.-A., Kim, B.K., Han, J.H., Park, T.S., Hwang, S., In Cho, S., Lee, W.-Y., Kim, Y.-R., 2010. Surface and Coatings Technology 205, S275–S278.
Kiani, A., Alpuche-Aviles, M.A., Eggers, P.K., Jones, M., Gooding, J.J., Paddon-Row, P.M.N., Bard, A.J., 2008. Langmuir 24, 2841–2849.
Liu, J.T., Chen, C.J., Ikoma, T., Yoshioka, T., Cross, J.S., Chang, S.-J., Tsai, J.-Z., Tanaka, J., 2011. Analytica Chimica Acta 703, 80–86.
Löfas, S., Whirter, M., 2006. The art of Immobilization for SPR Sensors. In: Homola, J., Wolfbeis, O.S. (Eds), Surface Plasmon Resonance Based Sensors, Springer Verlag, New York, pp. 3–44.
Lukes, J., Mauricio, I.L., Schonian, G., Dujardin, J.-C., Soteriadou, K., Dedet, J.-P., Kuhls, K., Tintaya, K.W.Q., Jirku, M., Chocholova, E., Haralambous, C., Pratlong, F., Obornik, M., Horak, A., Ayala, F.J., Miles, M.A., 2007. Proceedings of the National Academy of Sciences 104, 9375–9380.
Luz, R.C.S, Damos, F.S., Bof, A.O., Beck, J., Kubota, L.T., 2005. Electrochimica Acta 50, 2675–2683.
Mathers, C.D., Ezzati, M., Lopez, A.D., 2007. PLoS Neglected Tropical Diseases 2007, 1–114.

Mirkin, M.V., Fan, F.-R.F., Bard, A.J., 1992. Journal of Electroanalytical Chemistry 328, 47–62.
Moreno, J., Alvar, J., 2002. Trends in Parasitology 18, 399–405.
Murray, H.W, Berman, J.D., Davies, C.R., Clive, R., Saravia, N.G., 2005. The Lancet 366, 1561–1577.
Norlin, A., Pan, J., Leygraf, C., 2002. Biomolecular Engineering 19, 67–71.
Pei, R., Cheng, Z., Wang, E., Yang, X., 2001. Biosensors and Bioelectronics 16, 355–361.
Randles, J.E.B, 1947. Discussions of the Faraday Society 1, 11–19.
Reis, A.B., Martins-Filho, O.A., Teixeira-Carvalho, A., Carvalho, M.G., Mayrink, W., França-Silva, J.C., Giunchetti, R.C., Genaro, O., Corrêa-Oliveira, R., 2006. Research in Veterinary Science 81, 68–75.
Salmain, M., Ghasemi, M., Boujday, S., Spadavecchia, J., Técher, C., Val, F., Le Moigne, V., Gautier, M., Briandet, R., Pradier, C.-M., 2011. Biosensors and Bioelectronics 29, 140–144.
Srivastava, P., Dayama, A., Mehrotra, S., Sundar, S., 2011. Transactions of the Royal Society of Tropical Medicine and Hygiene 105, 1–6.
Teixeira-Neto, R.G., Giunchetti, R.C., Carneiro, C.M., Vitor, R.W., Coura-Vital, W., Quaresma, P.F., Ker, H.G., De Melo, L.A., Gontijo, C.M., Reis, A.B., 2010. Veterinary Parasitology 11, 248–257.
Venugopal, M., Arya, S.K., Chornokur, G., Bhansali, S., 2011. Sensors and Actuators A: Physical 172, 154–160.
Wei, C., Bard, A.J., Mirkin, M.V., 1995. Journal of Physical Chemistry 99, 16033–16042.
World Health Organization, 2010. WHO Technical Report Series 949, pp. 1–186.
Zhang, L., Zhang, J., Zhang, C.H., 2009. Biosensors and Bioelectronics 24, 2085–2090.